

Towards a comprehensive understanding of visible-light photogeneration of hydrogen from water using cobalt(II) polypyridyl catalysts†

Cite this: *Energy Environ. Sci.*, 2014, 7, 1477

R. S. Khayzer,^{†,ag} V. S. Thoi,^{‡,bd} M. Nippe,^{bd} A. E. King,^{bd} J. W. Jurs,^{bd} K. A. El Roz,^a J. R. Long,^{*be} C. J. Chang^{*bcd} and F. N. Castellano^{*a}

Homogeneous aqueous solutions of photocatalytic ensembles, consisting of $[\text{Ru}(\text{bpy})_3]^{2+}$ as a photosensitizer, ascorbic acid/ascorbate as the electron source, and 10 distinct Co^{2+} -based molecular catalysts, were evaluated for visible-light induced hydrogen evolution using high-throughput screening. The combined results demonstrate that Co^{2+} complexes bearing tetradentate ligands yield more active photocatalytic compositions than their congeners with pentadentate ligands while operating with high catalyst stability. Additionally, molecular Co^{2+} catalysts with *cis* open coordination sites appear to be significantly more active for hydrogen evolution than those with *trans* open sites. As evidenced by mass spectrometric analysis of the reactor headspace and associated deuteration experiments, the H_2 gas generated in all instances was derived from aqueous protons. One of the most promising *cis*-disposed Co^{2+} species, $[\text{Co}(\text{bpyPY2Me})(\text{CH}_3\text{CN})(\text{CF}_3\text{SO}_3)](\text{CF}_3\text{SO}_3)$ (**1**), engages in highly efficient hydrogen evolving photocatalysis, achieving a turnover number of 4200 (H_2/Co) and a turnover frequency of 3200 (H_2/Co per h) at pH 4 under simulated sunlight (AM 1.5G, 100 mW cm^{-2}) at room temperature. At equimolar concentrations of photosensitizer and **1**, the total hydrogen produced appears to be exclusively limited by the photostability of $[\text{Ru}(\text{bpy})_3]^{2+}$, which was observed to decompose into an $\text{Ru}(\text{bpy})_2$ -ascorbate adduct, as evidenced by HPLC and ESI-MS experiments. Lowering the operating temperature from 27 to 5 °C significantly attenuates bpy dissociation from the sensitizer, resulting in a net ~two-fold increase in hydrogen production from this composition. The primary electron transfer steps of this photocatalytic ensemble were investigated by nanosecond transient absorption spectroscopy. Photoexcited $[\text{Ru}(\text{bpy})_3]^{2+}$ undergoes reductive quenching by ascorbic acid/ascorbate ($k_q = 2.6 \times 10^7 \text{ M}^{-1} \text{ s}^{-1}$), releasing $[\text{Ru}(\text{bpy})_3]^+$ from the encounter solvent cage with an efficiency of $55 \pm 5\%$. In the presence of catalyst **1**, $[\text{Ru}(\text{bpy})_3]^+$ generated in the initial flash-quench experiment transfers an electron ($k_{\text{et}} = 2 \times 10^9 \text{ M}^{-1} \text{ s}^{-1}$) at an efficiency of $85 \pm 10\%$ to the catalyst, which is believed to enter the hydrogen evolution cycle subsequently. Using a combinatorial approach, all ten Co^{2+} catalysts were evaluated for their potential to operate under neutral pH 7.0 conditions. Catalyst **7**, $[\text{Co}(\text{PY4MeH}_2)(\text{CH}_3\text{CN})(\text{CF}_3\text{SO}_3)](\text{CF}_3\text{SO}_3)$, was revealed to be most promising, as its performance metrics were only marginally affected by pH and turnover numbers greater than 1000 were easily obtained in photocatalytic hydrogen generation. These comprehensive findings provide guidelines for the development of molecular compositions capable of evolving hydrogen from purely aqueous media.

Received 9th December 2013
Accepted 19th February 2014

DOI: 10.1039/c3ee43982h

www.rsc.org/ees

^aDepartment of Chemistry, North Carolina State University, Raleigh, NC 27695-8204, USA. E-mail: fncastel@ncsu.edu

^bDepartment of Chemistry, University of California, Berkeley, California 94720, USA. E-mail: chrischang@berkeley.edu; jrlong@berkeley.edu

^cDepartment of Molecular and Cell Biology, University of California, Berkeley, California 94720, USA

^dChemical Sciences Division, Lawrence Berkeley National Laboratory, Berkeley, California 94720, USA

^eMaterials Sciences Division, Lawrence Berkeley National Laboratory, Berkeley, California 94720, USA

^fHoward Hughes Medical Institute, University of California, Berkeley, California 94720, USA

^gDepartment of Natural Sciences, Lebanese American University, Chouran, Beirut 1102-2801, Lebanon

† Electronic supplementary information (ESI) available: Experimental section, high-throughput screening result of different compositions, ESI-MS and UV-vis analyses, quantum yield of hydrogen production, sensitizer luminescence quenching, transient absorption studies, spectroelectrochemistry and electrochemistry measurements, and X-ray structural parameters of catalysts **1**, **2**, **4**, and **6–9**. See DOI: 10.1039/c3ee43982h

‡ R.S.K. and V.S.T. contributed equally to this work.

Broader context

Renewable solar fuels represent alternative and environmentally friendly energy sources necessary for our planet's future. Hydrogen is a combustible gas that can be produced from proton reduction in water photocatalytically using visible solar photons. Since the combustion product of H₂ is water, this chemical conversion cycle represents one ideal scenario for the generation of clean and renewable energy. In the current manuscript, we describe homogeneous visible-light absorbing photocatalytic compositions consisting of the benchmark Ru(II) photosensitizer, [Ru(bpy)₃]²⁺, along with 10 different Co(II) polypyridyl catalysts that can produce copious amounts of hydrogen in pure water under solar flux in the presence of the sacrificial electron donor ascorbic acid/ascorbate. High-throughput photochemical screening and optimization along with the detailed mechanistic understanding of the photoactive portions of these compositions lay important groundwork for further development of this and related technologies.

1. Introduction

The development of photocatalytic systems intended to drive hydrogen evolution from water using visible light remains a challenging scientific problem.^{1–8} Inasmuch as there has been formidable recent progress spanning the gamut of relevant parameters—turnover number (TON), turnover frequency (TOF), total H₂ produced, quantum efficiency, H₂-evolving mechanisms, *etc.*—all homogenous-based ensembles eventually lose functionality due to decomposition of the molecular sensitizers and/or catalysts.^{9–12} In most instances, the fate of these molecules is ill-defined.^{13–15} The introduction of high-throughput photocatalytic screening of heterogeneous systems by the Bernhard group paved the way for the comprehensive evaluation of many relevant experimental parameters (solution composition, pH, sensitizer/catalyst concentrations, *etc.*), rapidly leading to the optimized conditions for H₂-evolving photocatalysis for a given composition.^{16–18} This combinatorial approach has been adopted by a number of research groups and rapidly led to record H₂-evolving photocatalytic metrics in both homogeneous and heterogeneous systems.^{19–21} It is important to note that given the limitations in sensitizer, catalyst, and sacrificial electron donor solubility/activity, most aqueous systems require the addition of non-innocent organic co-solvent(s) that markedly affect hydrogen production rates and yields. Since the primary motivation for H₂-producing catalysis is to reduce protons from water, organic additives and their waste by-products should be minimized or completely eliminated.

Owing to the poor solubility and aqueous activity of one or more of the necessary components, only a handful of homogeneous H₂-evolving photocatalysts have been evaluated in pure water.^{13,15,20,22–25} More recently, electro- and photochemical proton reduction catalysts based on iron,^{26–32} cobalt,^{33–41} nickel,^{42–46} and molybdenum^{47–49} centers have been shown to generate hydrogen from mixed organic–aqueous and aqueous media.^{50,51} The identification of aqueous-compatible molecular catalysts for hydrogen-evolution reactivity has permitted their translation into photocatalytic schemes. Alberto and coworkers recently realized significant TONs in acidified water using near-visible absorbing Re(I) metal-to-ligand charge transfer (MLCT) sensitizers ($\lambda_{\text{ex}} = 385 \text{ nm}$) in concert with cobalt-based tetra- and pentapyridyl catalysts.^{23,52} In addition, H₂ has now been generated from neutral water photocatalytically using both molecular and semiconducting visible light capturing sensitizers in conjunction with cobalt pentapyridine catalysts and ascorbate as the electron source.^{13,53} In these proof-of-principle

studies, the benchmark MLCT chromophore [Ru(bpy)₃]²⁺ was utilized as the molecular sensitizer, because it can be reductively quenched by ascorbate in water, as was first shown in the 1980s.¹⁵ These results set the stage for combinatorial optimization of homogeneous photocatalysis operating in water using newly conceived Co²⁺-based H₂ generating electrocatalysts.

The present investigation was motivated by the need to identify homogeneous compositions that function in pure water under visible-light illumination and to thoroughly understand key rate-controlling parameters and decomposition processes occurring under these conditions. The evaluated photocatalytic ensembles contain [Ru(bpy)₃]²⁺ as the photosensitizer, ascorbate as the sacrificial electron donor, and 10 distinct Co²⁺-based molecular catalysts, of which five bear newly-synthesized ligands. These molecules, nine of which bear tetradentate polypyridine ligands, are directly compared to the high performance pentadentate hydrogen evolution catalyst [(PY5Me₂)Co(H₂O)]²⁺. The tetradentate complexes are further discriminated by having open *cis* or *trans* coordination sites. High-throughput photocatalytic screening⁵⁴ was employed to compare these numerous systematically varied compositions and to seek individually optimized conditions for visible-light induced homogeneous photocatalytic H₂ generation. Catalyst **1** was found to be highly stable and produce copious amounts of H₂ under optimized conditions in pure water at pH 4. As a result, this particular composition was selected for detailed spectroscopic and mechanistic investigations. Hydrogen production with this ensemble was found to be solely limited by the photostability of the sensitizer, and was readily improved by lowering the reaction temperature, in essence attenuating the photosubstitution reaction with ascorbate. Transient absorption spectroscopy successfully identified the first two electron transfer intermediates generated during this aqueous photocatalysis, revealing the rate constants and cage escape efficiencies for these reactions, which ultimately lead to hydrogen evolution. Additionally, the high-throughput approach permitted rapid screening of numerous compositions, resulting in the identification of catalyst **7**, which is shown to operate efficiently at neutral pH 7.0 conditions.

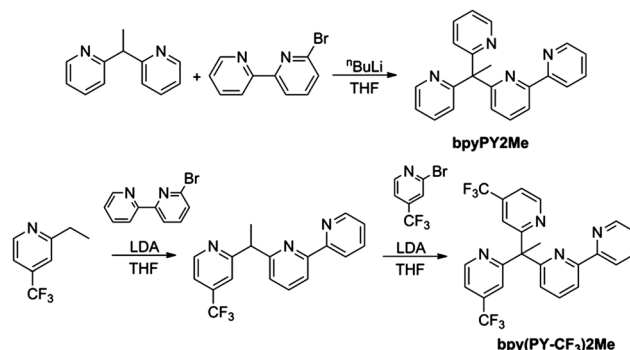
2. Results and discussion

The incorporation of redox-active bpy moieties into pentadentate ligand sets was recently shown to increase the efficiency of the corresponding Co catalysts for electro- and photocatalytic H₂ production.⁵³ The first part of this section comparatively evaluates photocatalytic ensembles utilizing Co complexes that

feature tetradentate, bpy-containing ligand sets and mechanistic details related to key electron transfer steps in the champion optimized composition using catalyst **1**. We then introduce three new Co catalysts bearing tetrapyridyl ligands, one of which (catalyst **7**) exhibits superior photocatalytic activity for hydrogen generation at neutral pH 7.0.

Design and synthesis of catalysts with bpy containing ligands

The identification of design criteria for the rational development of hydrogen evolution catalysts that are soluble, stable, and highly active in water represents an on-going challenge in the search for viable systems for homogeneous H₂ production. We utilized a high-throughput screening approach to comparatively evaluate six Co-based catalysts. Because a number of previously reported molecules are unable to function as catalysts at higher concentrations in aqueous solutions, we synthesized a new cobalt(II) compound, [Co(bpyPY2Me)(CH₃CN)(CF₃SO₃)](CF₃SO₃) (**1**), bearing 2-bis(2-pyridyl)(methyl)-methyl-6-pyridylpyridine (bpyPY2Me) as a ligand. To further investigate structure–function relationships, we also prepared catalyst **2** in which electron-withdrawing CF₃ groups have been incorporated into the 4-positions of both pyridine moieties in the new ligand bpy(PY-CF₃)₂Me. Such ligand modifications have been shown to have significant effects on catalytic performance.^{53,55} Catalyst **3** (Chart 1) was reported previously to be catalytically active in CH₃CN–H₂O mixtures, but is not soluble in neat water at millimolar concentrations.¹³ A very closely related cobalt complex was later utilized to produce H₂ photocatalytically from water.⁴¹ We prepared the corresponding Co²⁺ triflate compound **4** (Fig. S1†) and include it in this study for comparative purposes. Catalysts **1–4** share open *cis* coordination sites as a common design feature. Recently, the *trans* bis-



Scheme 1 Synthesis of the new ligands bpyPY2Me and bpy(PY-CF₃)₂Me.

aquo Co²⁺ complex of quaterpyridine (qpy) has been shown to be active for hydrogen evolution in water–solvent mixtures.³⁹ We therefore synthesized [Co(qpy)(OH₂)₂](ClO₄)₂ (**5**)⁵⁶ and a related new compound (**6**) bearing the more flexible ligand 1,3-di([2,2'-bipyridin]-6-yl)propane (pr-bpy₂)⁵⁷ (Fig. S2†), to extend further our structure–function analysis.

The syntheses of the new ligands are shown in Scheme 1. The ligand bpyPY2Me is readily accessible *via* lithiation of 1,1-bis(2-pyridyl)ethane followed by reaction with 6-bromo-2,2'-bipyridine. The ligand bpy(PY-CF₃)₂Me can be obtained in two steps *via* deprotonation/nucleophilic aromatic substitution reaction sequences. Complexation of bpyPY2Me and bpy(PY-CF₃)₂Me with Co(CH₃CN)₂(CF₃SO₃)₂ in CH₃CN is facile, and diethyl ether diffusion yields **1** and **2**, respectively, as crystalline solids.

The crystal structures of **1** and **2** are shown in Fig. 1 (see Tables S1 and S3† for detailed crystallographic information). The Co²⁺ centers in these structures display the expected distorted octahedral coordination geometry with exogenous ligands occupying *cis* coordination sites. The averaged Co–L bond lengths (2.11 Å in **1**; 2.10 Å in **2**) are indicative of a high-spin Co²⁺ ion with *S* = 3/2. Importantly, introduction of the CF₃ groups into the ligand weakens the pyridine–cobalt interactions significantly, as can be seen by the 0.029(5) Å elongated Co–N_{py} bond lengths in **2** as compared to **1**.

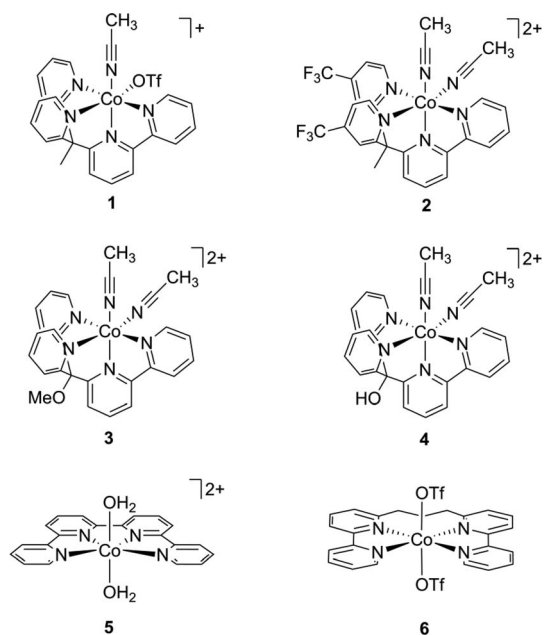


Chart 1 Evaluated Co²⁺ catalysts with tetradentate polypyridine ligands (OTf[−] = CF₃SO₃[−]).

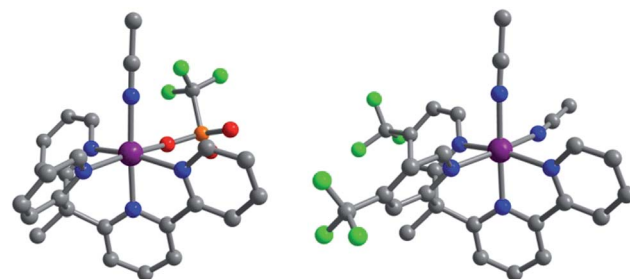


Fig. 1 Molecular structures of the mono- and dicationic Co²⁺ complexes in the crystal structures of **1** (left) and **2** (right), respectively. Purple, blue, grey, red, orange, and green spheres represent Co, N, C, O, S, and F atoms, respectively; H atoms have been omitted for clarity.

Catalytic activity

The design of integrated photocatalytic systems capable of producing H₂ requires an understanding of the energetics relevant to electron transfer between different species of the ensemble. Newly synthesized **1** and **2** were investigated both electro- and photochemically for their catalytic H₂ evolution activities. In order to rationalize the relative performance of these catalysts in aqueous media, we conducted cyclic voltammetry at equal cobalt concentrations (~0.3 mM) in 0.3 M H₂A/HA⁻ buffer at pH 4.0 chosen based on the high-throughput screening evaluation of different experimental conditions (Fig. S3–S5†). The cyclic voltammogram of **1** is unique under these conditions in that no pre-catalytic reduction feature was observed.⁵⁸ Instead, electrocatalytic current enhancement was observed at an onset potential of ~-0.9 V vs. NHE (Fig. 2a). We postulate that catalyst **1** can operate directly from its Co⁺ state and the Co^{2+/+} reduction occurs at this potential. The incorporation of CF₃ groups in **2** results in a small precatalytic feature at -0.75 V, which we assign to the Co^{2+/+} reduction. The 150 mV

positive shift in the Co^{2+/+} reduction potential in **2** from that of **1** suggests that Co⁺ is more strongly stabilized in **2**. However, the catalytic currents at more negative potentials for **2** are strongly attenuated, indicating lower activity of **2** as compared to **1** for hydrogen evolution at potentials more negative than -0.9 V vs. NHE. Previous reports have shown that the introduction of electron-withdrawing groups in similar polypyridyl Co complexes have led to diminished reactivity of the corresponding Co⁺ species.^{53,55,59} Importantly, the findings of these initial electrochemical investigations are confirmed by results of photocatalytic experiments, as will be discussed below.

Fig. 2b shows the amounts of H₂ evolved utilizing [Ru(bpy)₃]²⁺ as the photosensitizer and catalysts **1**–**6** with 0.3 M H₂A/HA⁻. In agreement with the electrochemical studies, photocatalytic experiments utilizing **1** generated a five-fold increase in H₂ production as compared to **2**. Interestingly, the presence of the CH₃ group in the ligand backbone of catalyst **1** instead of the previously reported OMe group in **3** or OH group in **4** also results in greatly enhanced catalytic activity (almost two-fold). This remarkable sensitivity of the catalytic performance on such subtle ligand modifications highlights the importance of systematic studies to elucidate structure–activity relationships. Another key observation is that utilization of complexes **5** and **6** results in significantly attenuated amounts of photogenerated H₂, suggesting a beneficial effect of open *cis* (**1**–**4**) over *trans* (**5** and **6**) coordination sites. We believe that the specific optimized pH value for each catalyst is due to the relative basicity of the corresponding Co(i) catalyst that is presumably protonated in the hydrogen evolution cycle.

The homogeneity of the photocatalytic system utilizing **1** was ascertained through several independent experiments. The Hg (0.1 mL) poisoning test showed no significant changes of the photocatalytic rate of hydrogen produced (Fig. S6†).^{60,61} Dynamic light scattering studies before and after photocatalysis indicated no detectable formation of nanoparticles (Fig. S7†). Additionally, a linear dependence on the number of moles of hydrogen produced with respect to the concentration of each component was observed (Fig. S8†). All of these findings strongly suggest a molecular catalyst for the photocatalytic hydrogen production in each of the present cases.

Turnover numbers (TONs) per mole of **1** were assessed at different concentrations of **1** (Fig. 3). As anticipated, increasing the amount of catalyst in the homogenous mixture results in concomitant scaling of the total amount of hydrogen generated with time (Fig. 3a), maximizing at 20 μM of **1**. Furthermore, the TON dramatically increases with decreasing cobalt concentration, achieving values greater than 10 000 (H₂/Co) at sub-micromolar concentrations (Fig. 3b). These TONs are among the highest reported to date for photocatalytic H₂ evolution in pure water and are comparable to the values reported by Alberto and coworkers on systems utilizing UV light.²³ It is important to note that the highest TONs for a given catalyst are typically observed at very low catalyst concentrations wherein catalyst stability is limiting. However, the total amount of hydrogen produced is often insignificant for any practical application since these reaction conditions do not yield combustible quantities of H₂ gas. Here, we stress the importance of

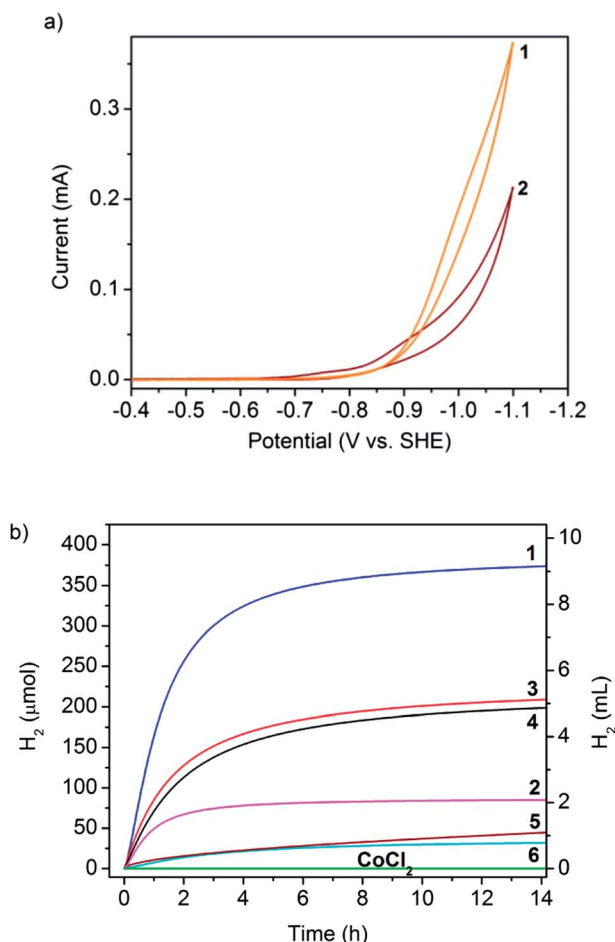
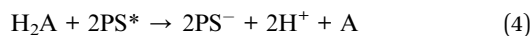
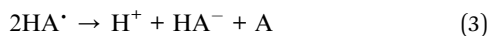
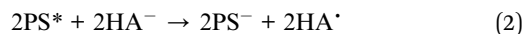


Fig. 2 (a) Cyclic voltammograms of **1** and **2** (0.2 mM) in aqueous solution containing 0.3 M H₂A/HA⁻ at pH 3.95 ($\nu = 100 \text{ mV s}^{-1}$) (b) photocatalytic hydrogen production under 452 ± 10 nm (540 mW) of a solution containing 2 × 10⁻⁵ M **1** (blue, pH 4), **2** (magenta, pH 4.5), **3** (red, pH 4.5), **4** (black, pH 4), **5** (brown, pH 5.5), **6** (light blue, pH 5.0) or CoCl₂ control (green, pH 4), 3.3 × 10⁻⁴ M [Ru(bpy)₃]²⁺ in 0.3 M H₂A/HA⁻.

The ground and excited state redox potentials for $[\text{Ru}(\text{bpy})_3]^{2+}$ in water are well established.⁶² Ascorbic acid (H_2A) oxidation to dehydroascorbate (A) ($\text{H}_2\text{A} \rightarrow \text{A} + 2\text{e}^- + 2\text{H}^+$) coupled with hydrogen production represents a total energy storage process of 0.41 V at pH 4.0 (eqn (1)–(4) and Scheme 2).^{14,15,22} In the pH range of 2.5–4.0, HA^\bullet was found to disproportionate to HA^- and A , eqn (3).^{22,63} Dehydroascorbate is usually hydrated and subsequently converted to other species. Eisenberg and coworkers have identified the decomposition products of H_2A by ^1H and ^{13}C NMR, and found that the hydrated dehydroascorbate oxidation product dominates under photocatalytic conditions.²⁰ From the relevant energetics presented in Scheme 2, $[\text{Ru}(\text{bpy})_3]^{2+*}$ (excited state reduction potential $\sim +0.84$ V) can be reductively quenched by $\text{H}_2\text{A}/\text{HA}^-$ (ascorbate oxidation potential $\sim +0.17$ V) while it is thermodynamically unfavorable for this excited state to be oxidatively quenched by catalyst **1**. Subsequent to reductive quenching by ascorbate, the one-electron reduced $[\text{Ru}(\text{bpy})_3]^+$ species (~ -1.26 V potential) is now thermodynamically poised to deliver this more energetic electron to **1** in a dark reaction. As evidenced by the electrochemical data presented in Fig. 2a, the resultant Co^+ species is then capable of evolving H_2 directly.



Photochemical behavior

The photostability of the ensemble containing **1** was examined by UV-vis spectroscopy and LC-MS to glean insight into the nature of the ultimate degradation products. An HPLC study of the reaction mixture before and after catalysis indicated that the cobalt species is more stable than the photosensitizer (Fig. S9†). The major $[\text{Ru}(\text{bpy})_3]^{2+}$ decomposition product was determined to be $[\text{Ru}(\text{bpy})_2\text{HA}]^+$ on the basis of UV-vis and ESI-MS studies (Fig. S10†). Minor side-products such as $[\text{Ru}(\text{bpy})_2(\text{H}_2\text{O})_2]^{2+}$ resulting from bipyridine ligand substitution are also plausible degradation species. At equimolar concentrations of **1** and $[\text{Ru}(\text{bpy})_3]^{2+}$ (2×10^{-5} M), the limitation imposed by the photostability of the Ru(II) sensitizer was demonstrated by successful regeneration of hydrogen production through the addition of fresh aliquots of $[\text{Ru}(\text{bpy})_3]^{2+}$ after catalysis had ceased (Fig. 5). Significantly, the addition of any other single component to the system failed to regenerate photocatalytic activity.

The established mechanism for dechelation of bipyridine from $[\text{Ru}(\text{bpy})_3]^{2+}$ involves the population of the thermally accessible ligand field states that arise after photoexcitation.^{64–67} For $1/[\text{Ru}(\text{bpy})_3]^{2+}$ in pH 4.0 water, control experiments confirmed that the decomposition required light as fresh mixtures of these components were stable for days in the dark at ambient temperature. Furthermore, HA^- acts as both quencher

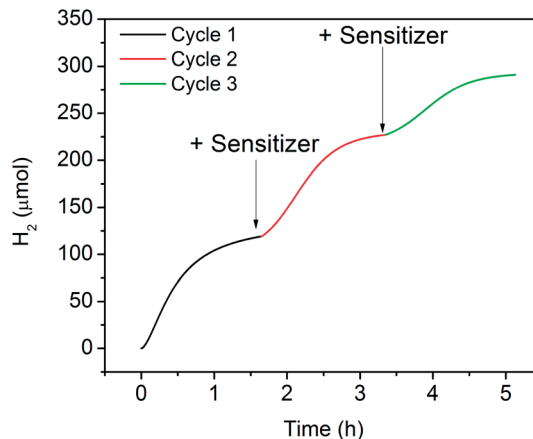


Fig. 5 Regeneration of photocatalytic hydrogen production resulting from the addition of fresh aliquots of $[\text{Ru}(\text{bpy})_3]^{2+}$. Photocatalysis was induced using blue LED excitation centered at 452 nm. Conditions: 2×10^{-5} M **1**, 2×10^{-5} M $[\text{Ru}(\text{bpy})_3]^{2+}$ and 0.3 M $\text{H}_2\text{A}/\text{HA}^-$ at pH 4.

and potential ligand, and the presumed $[\text{Ru}(\text{bpy})_2\text{HA}]^+$ degradation product competitively absorbs visible excitation photons in the blue. We estimated an extinction coefficient of $6000 \text{ M}^{-1} \text{ cm}^{-1}$ for this species at 452 nm from the UV-vis absorption spectrum of $[\text{Ru}(\text{bpy})_3]^{2+}$ ($\epsilon = 14\,500 \text{ M}^{-1} \text{ cm}^{-1}$) before and after the photoreaction (Fig. S11†). This undesirable byproduct inhibits the complete regeneration of catalysis following the addition of fresh photosensitizer at high concentrations due to the competitive absorbance of incident photons as depicted by the decreased catalytic activity upon the addition of a fresh aliquot of photosensitizer in the second regeneration cycle *versus* the first one, Fig. 5.

The overall amount of hydrogen accumulated in the headspace increased with decreasing temperature, and was accompanied by slower initial rates of hydrogen generation (Fig. 6). The slight decrease in the rate of hydrogen production at lower temperatures is attributed to slower rates of the various

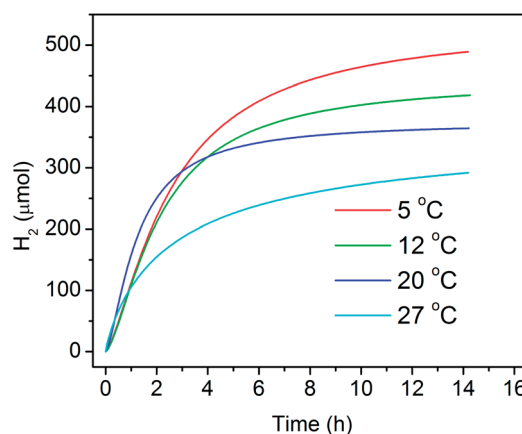


Fig. 6 Kinetics of photocatalytic hydrogen production performed at different temperatures under blue LED excitation centered at 452 nm. Conditions: 2×10^{-5} M **1**, 3.3×10^{-4} M $[\text{Ru}(\text{bpy})_3]^{2+}$ and 0.3 M $\text{H}_2\text{A}/\text{HA}^-$ at pH 4.

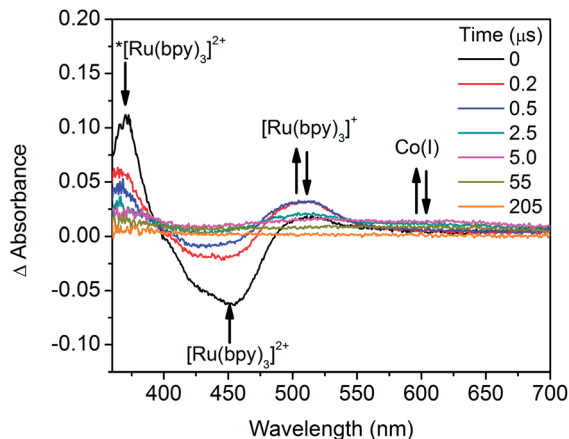


Fig. 7 Transient absorption difference spectra of a solution containing 2.9×10^{-4} M **1** and 2.5×10^{-5} M $[\text{Ru}(\text{bpy})_3]^{2+}$ in 0.3 M $\text{H}_2\text{A}/\text{HA}^-$ at pH 4, recorded at the specified delay times following nanosecond laser excitation at 452 nm.

reactions involved in the hydrogen production cycle. Similarly, increasing the temperature even slightly above room temperature (27 °C) imparted detrimental effects to the photoinduced generation of H_2 from this mixture, consistent with the activation of ligand-field states promoting substitution chemistry. These findings elucidate the importance of temperature control in the photocatalytic hydrogen production measurements utilizing $[\text{Ru}(\text{bpy})_3]^{2+}$ and related molecules as photosensitizers. The photosensitizer's decomposition was the main contributor to the cease of hydrogen evolution at high catalyst concentrations whereas the catalyst decomposition is often limiting the performance at low catalyst concentration as observed in Fig. 3 and 7.

Electron transfer processes

High-throughput optimization revealed the key experimental parameters necessary to achieve idealized photoinduced hydrogen production in the champion composition. These results provided the impetus for a detailed investigation into the initial electron transfer reactions driving this photochemistry. A series of static and dynamic spectroscopic measurements were performed to elucidate the electron transfer yields and dynamics of this ensemble. Selective excitation of $[\text{Ru}(\text{bpy})_3]^{2+}$ in water quantitatively yields $^3[\text{Ru}(\text{bpy})_3]^{2+*}$ possessing a 0.6 μs lifetime (Fig. S13[†]), rendering it susceptible to electron transfer quenching.^{68–70} This excited state is reductively quenched by $\text{H}_2\text{A}/\text{HA}^-$ in water at pH 4.0 with a bimolecular rate constant of $k_{\text{q}} = 2.6 \times 10^7 \text{ M}^{-1} \text{ s}^{-1}$, as determined using dynamic Stern–Volmer luminescence quenching (Fig. S14[†]). Under optimized conditions and in the absence of any cobalt catalyst, the one-electron reduced ruthenium species $[\text{Ru}(\text{bpy})_3]^+$ ($\epsilon_{505\text{nm}} = 1.2 \times 10^4 \text{ M}^{-1} \text{ cm}^{-1}$, Fig. S15[†]) quantitatively recombines with the oxidized ascorbate (HA^\cdot) species, as ascertained by nanosecond transient absorption spectroscopy, $\lambda_{\text{ex}} = 452 \text{ nm}$ (Fig. S16[†]). Excited state absorption spectroscopy performed on this reaction under flash-quench conditions

permits the yield of charge-separated products (cage escape yield) to be determined using relative actinometry, as previously described.^{71,72} The cage escape yield for the initially formed $[\text{Ru}(\text{bpy})_3]^+/\text{HA}^\cdot$ pair was estimated to be 0.55 ± 0.05 and is in quantitative agreement with the previously reported value (Fig. S16[†]).¹⁵ In essence, only 55% of the total initial photoinduced electron transfer products are available for subsequent reaction. This represents a significant loss mechanism mandating future development of alternative water-soluble sensitizer/donor combinations.

The addition of catalyst **1** to the flash-quench mixture followed by excitation with 452 nm laser pulses markedly accelerates the disappearance of the initially formed $[\text{Ru}(\text{bpy})_3]^+$ species (Fig. 7). This coincided with the generation of a new species possessing a weak and broad absorption transient between 450 and 700 nm (Fig. 7). These transient features are consistent with a dark electron transfer reaction from $[\text{Ru}(\text{bpy})_3]^+$ to $\text{Co}(\text{II})$, forming $\text{Co}(\text{I})$ and regenerating the resting state of the sensitizer. Evidence for the generation of the $\text{Co}^{\text{I}}(\text{bpyPY2Me})$ species in laser flash photolysis was supported by spectroelectrochemistry experiments (Fig. S17, [†] $\text{Co}(\text{I}) \epsilon_{505\text{nm}} = 5500 \text{ M}^{-1} \text{ cm}^{-1}$). It is this $\text{Co}(\text{I})$ species which is generally considered the crucial intermediate in the hydrogen evolution cycle in macrocyclic cobalt catalysts.^{11,12,36,73}

The pseudo-first order rate constant of the reaction between the reduced photosensitizer and this cobalt catalyst was calculated from an analysis of transient absorption kinetics under flash-quench conditions (Fig. 8). The transient decay data for the $[\text{Ru}(\text{bpy})_3]^+$ species measured at 505 nm as a function of catalyst concentration are presented in Fig. 8a. Fitting the initial portion of the decay data with a sum of 2 exponential functions permitted the extraction of the rate that systematically varied with the concentration of **1** under pseudo-first order conditions. Plotting these rates *versus* catalyst concentration yielded a straight line with a slope of $2 \times 10^9 \text{ M}^{-1} \text{ s}^{-1}$ (Fig. 8b). This electron transfer rate constant is comparable to that obtained by Alberto and coworkers using transient infrared spectroscopy in a system composed of $\text{H}_2\text{A}/\text{HA}^-$ electron donor, $\text{Re}(\text{I})$ carbonyl photosensitizer, and **4** as a catalyst.²³ We also estimated the cage escape yield for the $[\text{Ru}(\text{bpy})_3]^{2+}/\text{Co}^{\text{I}}(\text{bpyPY2Me})$ pair to be 0.85 ± 0.10 . Taken together, these two electron transfer efficiencies suggest the upper quantum efficiency limit of catalysis in this composition to be 47%, albeit by completely ignoring all remaining steps of the hydrogen evolution reaction. Since the measured quantum yield for H_2 evolution was 7.5%, it becomes clear that these initial electron transfer reactions are not limiting the overall performance metrics.

The $\text{Co}^{\text{I}}(\text{bpyPY2Me})$ moiety absorbs across the entire range of the visible spectrum as evidenced by the transient difference spectrum obtained beyond a 10- μs delay (Fig. 7). The cobalt catalyst is the only species possessing a difference spectrum at this point in time, as $[\text{Ru}(\text{bpy})_3]^{2+}$ reforms subsequent to electron transfer and $\text{H}_2\text{A}/\text{HA}^-$ along with any associated oxidation products do not possess any visible light absorbing features (Fig. 7). The apparent lifetime of the Co^{I} species is approximately 60 μs at 2.9×10^{-4} M **1**, 2.5×10^{-5} M $[\text{Ru}(\text{bpy})_3]^{2+}$, and 0.3 M $\text{H}_2\text{A}/\text{HA}^-$ at pH 4.0. This time constant was determined

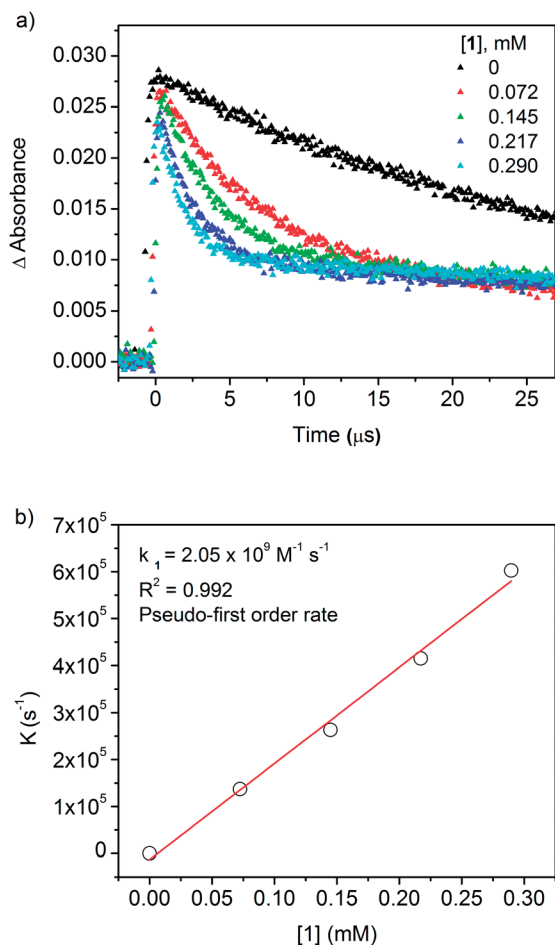


Fig. 8 (a) Absorption transients monitored at 505 nm, where both $[Ru(bpy)_3]^+$ and $Co^I(bpyPY2Me)$ absorb. (b) Rate of the reaction between $[Ru(bpy)_3]^+$ and $Co^{II}(bpyPY2Me)$ versus the concentration of the catalyst. Conditions: $2.5 \times 10^{-5} M$ $[Ru(bpy)_3]^{2+}$ in $0.3 M$ H_2A/HA^- at pH 4.

from both the long-lived component of the biexponential decay at 505 nm and the single exponential kinetics measured at 650 nm, where the Co^+ species absorbs exclusively (Fig. S18[†]). As previously highlighted, Co^+ formation and subsequent protonation to yield a cobalt hydride represent essential steps leading to hydrogen evolution.³⁶ The invariant UV-vis absorption spectrum measured before and after the laser flash photolysis experiments confirm that no significant decomposition of $[Ru(bpy)_3]^{2+}$ occurs during the course of those experiments. Decomposition of the sensitizer was, however, observed during long-term continuous photolysis under large luminous flux.

To identify the source of protons in the ultimate hydrogen product, experiments utilizing deuterated water were undertaken. Replacement of H_2O with D_2O results in >90% deuterium incorporation (1% H_2 , 15% HD, 84% D_2) in the photoreactor headspace, with D_2 being the major product (Fig. 9a). The small amount of H-incorporation, predominantly as HD, was attributed to proton exchange between the initial H_2A , its decomposition products, and D_2O . The small hydrogen gas background measured from the headspace of solutions in the absence of the

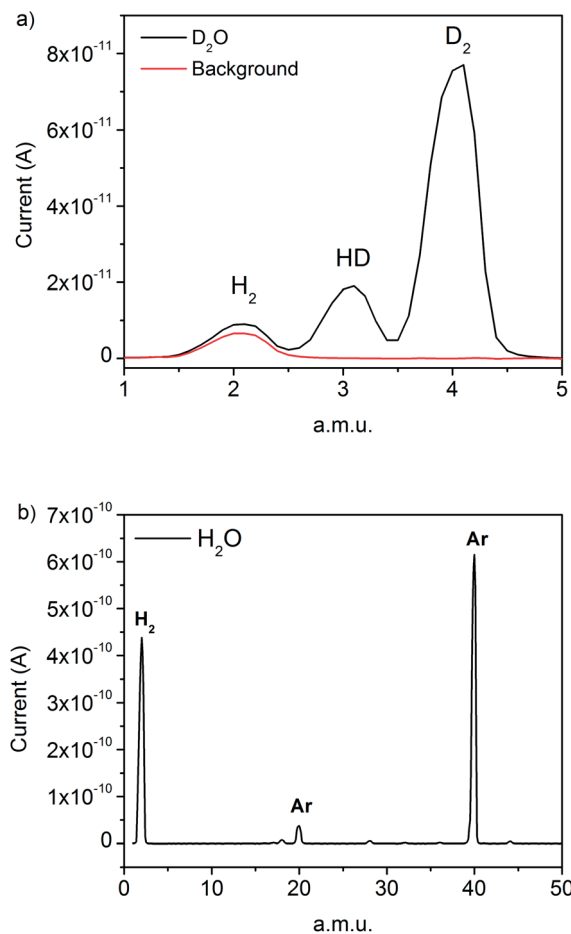


Fig. 9 (a) Mass spectrum of the analyzed headspace in the deuteration experiments (black) after photocatalysis ceases, along with the background (red) resulting from MS outgassing. The photocatalysis was induced using blue LED excitation centered at 452 nm. Conditions: $2 \times 10^{-5} M$ of **1**, $3.3 \times 10^{-4} M$ $[Ru(bpy)_3]^{2+}$ in $0.1 M$ H_2A/HA^- in D_2O at pD = 4.0. (b) Mass spectrum of the analyzed headspace in the presence of H_2O . Conditions: $2 \times 10^{-5} M$ **1**, $3.3 \times 10^{-4} M$ $[Ru(bpy)_3]^{2+}$ in $0.3 M$ H_2A/HA^- at pH 4.0 in H_2O .

photosensitizer-catalyst mixture results from spectrometer outgassing (Fig. 9a, red line). When the headspace of the reaction was analyzed by MS in the presence of water, H_2 was the major product formed during the course of catalysis (Fig. 9b). Taken together, these data clearly demonstrate that the hydrogen evolved is not a by-product of direct H_2A dehydrogenation and that the source of protons is indeed water.

Synthesis of $Co(II)$ catalysts with tetrapyrroline ligands and evaluation under neutral pHs

The foregoing results demonstrate that molecular Co^{2+} complexes of tetradentate, bpy-containing ligands can act as efficient catalysts for hydrogen evolution in aqueous media and have comparable stability with respect to their pentadentate congeners.⁵³ In fact, the two open *cis* coordination sites in **1** as compared to only one in a closely related Co^{2+} complex of the pentadentate ligand bpy_2PYMe ⁵³ renders **1** more active for H_2 evolution. We therefore decided to investigate the apparent

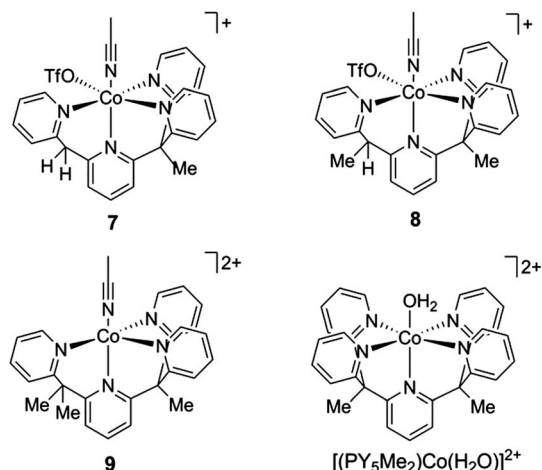


Chart 2 Tetrapyrrolyl and pentapyrrolyl Co^{2+} catalysts (OTf = CF_3SO_3^-).

beneficial effect of additional open coordination sites by synthesizing a series of Co^{2+} complexes of tetradentate pyridine ligands that are related to the redox inert pentadentate ligand PY5Me_2 . Chart 2 presents the chemical structures of the Co^{2+} complexes of the newly conceived ligands $\text{PY4Me}_2\text{H}$ (7), PY4Me_2 (8), and PY4Me_3 (9), as well as the earlier reported pentadentate reference catalyst $[(\text{PY5Me}_2)\text{Co}(\text{H}_2\text{O})]^{2+}$.

Synthetic access to these new ligands is readily given by a modular approach in which lithiation of an alkyl pyridine is followed by addition of a halogenated tripyridine precursor, PY3F^{74} (Scheme 3). Complexation of the ligands with $\text{Co}(\text{CF}_3\text{SO}_3)_2(\text{CH}_3\text{CN})_2$ in CH_3CN proceeds smoothly to yield Co complexes 7–9.

The solid-state structures of 7–9 are shown in Fig. 10. In all cases, the cobalt(II) center is coordinated by four pyridyl donors. The complexes in 7 and 8 also feature an equatorial CF_3SO_3^- anion and an axial solvent molecule to give a distorted octahedral geometry, while the complex in 9 exhibits square pyramidal coordination with a single acetonitrile ligand in basal position. Upon closer inspection, the coordination environment

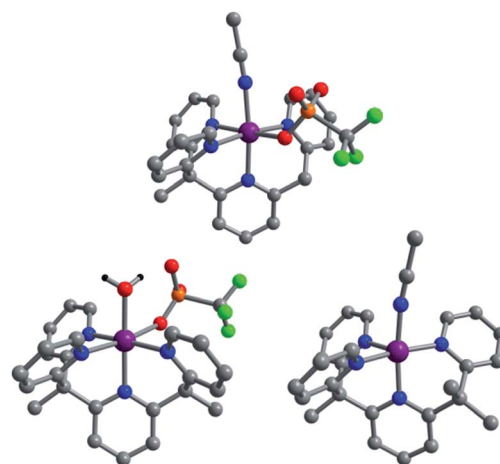
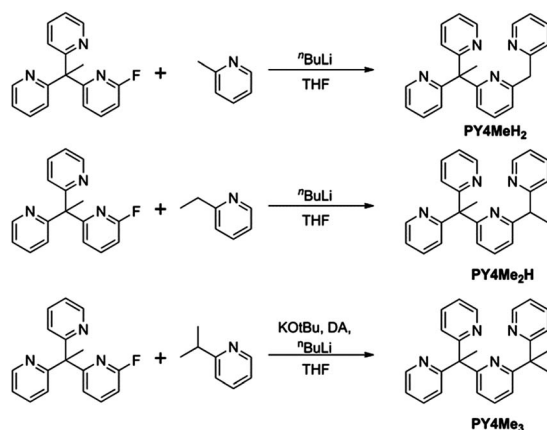


Fig. 10 Molecular structures of the mono- and dicationic Co^{2+} complexes in the crystal structures of 7 (top), 8 (left), and 9 (right), respectively. Purple, blue, grey, red, orange, and green spheres represent Co, N, C, O, S, and F atoms, respectively; hydrogen atoms (other than for H_2O in 6) have been omitted for clarity.

of Co^{2+} in 9 is sterically more congested compared to those of 7 and 8, with a methyl group situated ~ 2.9 Å away from the metal center, hindering binding of a sixth ligand (Tables S2 and S4[†]). We note that electron density corresponding to the H atoms of the proximal methyl group could be located and refined, providing a closest Co–H contact of 2.185 Å. The geometry around the metal center in 9 can thus be described by the angles formed by $\text{N}_{\text{py,eq}}\text{--Co--H}$ (83.89° , 85.73° , 170.58°) and $\text{N}_{\text{py,ax}}\text{--Co--H}$ (82.40°), closely resembling a pseudooctahedral coordination sphere despite ligation by only one solvent molecule. The steric effects of methyl groups in this equatorial site are also observed in the analogous site in 8. The Co–O(O_2SCF_3) bond length in 8 is 2.314(1) Å and is ~ 0.124 Å longer than the Co–O(O_2SCF_3) distance of 2.190(1) Å in 7. The weaker Co–O interaction in 8 suggests that even the presence of one methyl group near the equatorial site of interest can affect the binding of a sixth ligand.

We evaluated the three new complexes for their ability to act as hydrogen evolution electro- and photocatalysts. The high-throughput approach described above was utilized to identify optimized conditions with $[\text{Ru}(\text{bpy})_3]^{2+}$ as the sensitizer in photocatalytic experiments. Results from the pH dependence of H_2 evolution for catalysts 7–9 and the earlier reported $[(\text{PY5Me}_2)\text{Co}(\text{H}_2\text{O})]^{2+}$ complex are given in Fig. 11. Catalyst 7, bearing the least sterically demanding ligand, clearly outperforms 8, 9, and $[(\text{PY5Me}_2)\text{Co}(\text{H}_2\text{O})]^{2+}$ over the investigated pH range, with the optimal pH being 5. In stark contrast to the other catalysts investigated, 7 remains very active up to pH 7.5, albeit with attenuated amounts of produced H_2 with respect to lower pH.

Despite the many examples of electrocatalytic hydrogen generation by both homogeneous and heterogeneous systems, there are far fewer systems that can perform photocatalytic proton reduction in pure water at neutral pH with high turnover values.¹³ As such, catalyst 7 is a privileged motif that has important implications for environmentally benign, solar-



Scheme 3 Synthesis of ligands PY4Me_2 , $\text{PY4Me}_2\text{H}$, and PY4Me_3 .

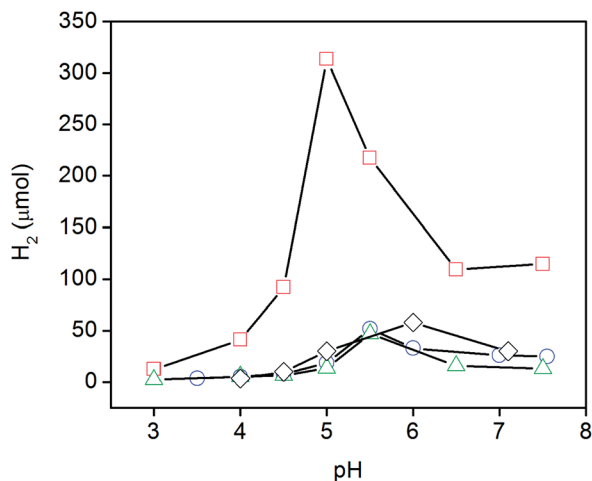


Fig. 11 Photocatalytic H₂ production in the presence of 2×10^{-5} M of complex 7 (red squares), 8 (blue circles), 9 (green triangles), and [CoPY5Me₂]²⁺ (black diamonds) in a 0.3 M H₂A/HA⁻ aqueous solution at pH 3 to 7.5 containing 3.3×10^{-4} M [Ru(bpy)₃]²⁺ under an inert atmosphere.

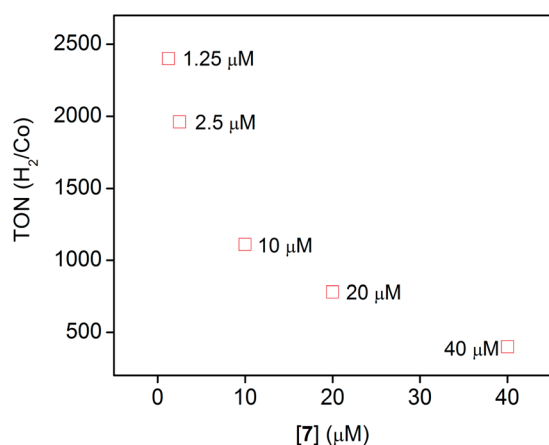


Fig. 12 TONs measured as a function of concentration of 7 in 0.3 M ascorbate in water at pH 7 containing 3.3×10^{-4} M [Ru(bpy)₃]²⁺ under an inert atmosphere.

driven hydrogen production. Based on these results, we suggest that the increased accessibility and greater number of open, labile coordination sites in 7 compared to the more sterically encumbered tetrapyrroline PY4 and pentapyridine PY5Me₂ analogs may aid the binding and transformation of H₂O substrates and H₂ products.

The observed high activity for water reduction at pH 7 for photocatalytic systems employing 7 warranted further investigation. Similar to the results obtained for 1 (see above), the H₂ production scales with the concentration of 7 and [Ru(bpy)₃]²⁺ at conditions where catalyst activity and light absorption are limiting (Fig. S22 and S23,† respectively). More importantly, 7 catalyzes water reduction remarkably well at neutral pH, with TONs over 1000 (H₂/Co) at low catalyst concentration (Fig. 12).

3. Conclusions

High-throughput screening allowed for extensive comparative evaluations of photocatalytic compositions intended for aqueous hydrogen evolution using visible light. These systems were composed of [Ru(bpy)₃]²⁺ as a photosensitizer, ascorbate/ascorbic acid as the electron source, and molecular Co²⁺ catalysts. Ten distinct Co²⁺ based catalysts were investigated and numerous conclusions can be drawn: (1) utilization of catalyst 1 allows for highly efficient hydrogen evolving photocatalytic systems in water, achieving 4200 (H₂/Co) turnovers and a turnover frequency of 3200 (H₂/Co per h) under simulated sunlight (AM 1.5, 100 mW cm⁻²) at room temperature and pH 4. The ultimate amounts of H₂ produced were limited solely by photosensitizer stability, not decomposition processes within the molecular catalyst. The product of the sensitizer decomposition has also been identified. (2) Catalysts of tetradentate ligands exhibited higher activity than their congeners with pentadentate ligands without losses in stability, as exemplified by direct comparisons to the champion pentadentate Co²⁺ hydrogen evolution catalyst [(PY5Me₂)Co(H₂O)]²⁺. (3) Tetradentate ligands that enforce open *cis* coordination sites yield significantly more active catalysts for hydrogen evolution than those that favor *trans* sites. (4) The newly conceived catalyst 7 is a rare example of a molecular species that remains significantly active for hydrogen evolution at neutral pH thereby enabling biocompatibility. (5) The majority of the H₂ generated in these homogeneous molecular-based photocatalysis experiments have their origin in aqueous protons.

Key electron transfer steps of the photocatalytic ensembles were thoroughly investigated by transient absorption spectroscopy. Photoexcited [Ru(bpy)₃]²⁺ undergoes reductive quenching by H₂A/HA⁻ ($k_q = 2.6 \times 10^7$ M⁻¹ s⁻¹), releasing [Ru(bpy)₃]⁺ from the encounter solvent cage with an efficiency of $55 \pm 5\%$. In the presence of catalyst 1, [Ru(bpy)₃]⁺ generated in the initial flash-quench experiment transfers an electron to 1 ($k_{et} = 2 \times 10^9$ M⁻¹ s⁻¹) at an efficiency of $85 \pm 10\%$, which is believed to enter the hydrogen evolution cycle subsequently. These combined findings provide insights into the development of molecular compositions capable of hydrogen evolution in aqueous media without the need of organic co-solvents.

Acknowledgements

This work was supported by DOE/LBNL Grant 403801 (C.J.C.), NSF grant CHE-1111900 (J.R.L.), and NSF grant CHE-1012487 (F.N.C.). V.S.T. thanks Profs. T. Don Tilley and Richard Andersen for insightful discussions as well as the National Science Foundation for a graduate fellowship. We acknowledge Babatunde S. Olaiya for considerable help with photocatalytic experiments. C.J.C. is an Investigator with the Howard Hughes Medical Institute.

References

- 1 H. B. Gray and A. W. Maverick, *Science*, 1981, **214**, 1201.
- 2 A. F. Heyduk and D. G. Nocera, *Science*, 2001, **293**, 1639.

- 3 *Energy resources through photochemistry and catalysis*, ed. M. Gratzel, Academic Press, New York, 1983.
- 4 *Photochemical Energy Conversion*, ed. J. R. Norris Jr and D. Meisel, Elsevier, New York, 1989.
- 5 A. J. Esswein and D. G. Nocera, *Chem. Rev.*, 2007, **107**, 4022.
- 6 *Homogeneous Photocatalysis*, ed. M. Chanon, John Wiley & Sons, Chichester, UK, 1997.
- 7 *Photoinduced Electron Transfer*, ed. M. A. Fox and M. Chanon, Elsevier, Amsterdam, 1988.
- 8 *Photogeneration of Hydrogen*, ed. A. Harriman and M. A. West, Academic Press, London, 1982.
- 9 M. Wang, L. Chen and L. Sun, *Energy Environ. Sci.*, 2012, **5**, 6763.
- 10 P. Du and R. Eisenberg, *Energy Environ. Sci.*, 2012, **5**, 6012.
- 11 V. S. Thoi, Y. Sun, J. R. Long and C. J. Chang, *Chem. Soc. Rev.*, 2013, **42**, 2388.
- 12 V. Artero, M. Chavarot-Kerlidou and M. Fontecave, *Angew. Chem., Int. Ed.*, 2011, **50**, 7238.
- 13 Y. Sun, J. Sun, J. R. Long, P. Yang and C. J. Chang, *Chem. Sci.*, 2013, **4**, 118.
- 14 W. R. McNamara, Z. Han, C.-J. Yin, W. W. Brennessel, P. L. Holland and R. Eisenberg, *Proc. Natl. Acad. Sci. U. S. A.*, 2012, **109**, 15594.
- 15 C. V. Krishnan and N. Sutin, *J. Am. Chem. Soc.*, 1981, **103**, 2141.
- 16 J. I. Goldsmith, W. R. Hudson, M. S. Lowry, T. H. Anderson and S. Bernhard, *J. Am. Chem. Soc.*, 2005, **127**, 7502.
- 17 M. S. Lowry, W. R. Hudson, R. A. Pascal and S. Bernhard, *J. Am. Chem. Soc.*, 2004, **126**, 14129.
- 18 L. L. Tinker, N. D. McDaniel, P. N. Curtin, C. K. Smith, M. J. Ireland and S. Bernhard, *Chem.-Eur. J.*, 2007, **13**, 8726.
- 19 T. M. McCormick, B. D. Calitree, A. Orchard, N. D. Kraut, F. V. Bright, M. R. Detty and R. Eisenberg, *J. Am. Chem. Soc.*, 2010, **132**, 15480.
- 20 Z. Han, F. Qiu, R. Eisenberg, P. L. Holland and T. D. Krauss, *Science*, 2012, **338**, 1321.
- 21 M. Elvington, J. Brown, S. M. Arachchige and K. J. Brewer, *J. Am. Chem. Soc.*, 2007, **129**, 10644.
- 22 G. M. Brown, B. S. Brunschwig, C. Creutz, J. F. Endicott and N. Sutin, *J. Am. Chem. Soc.*, 1979, **101**, 1298.
- 23 M. Guttentag, A. Rodenberg, C. Bachmann, A. Senn, P. Hamm and R. Alberto, *Dalton Trans.*, 2012, **42**, 334.
- 24 B. Probst, M. Guttentag, A. Rodenberg, P. Hamm and R. Alberto, *Inorg. Chem.*, 2011, **50**, 3404.
- 25 F. Wang, W. G. Wang, X. J. Wang, H. Y. Wang, C. H. Tung and L. Z. Wu, *Angew. Chem., Int. Ed.*, 2011, **50**, 3193.
- 26 R. Mejia-Rodriguez, D. Chong, J. H. Reibenspies, M. P. Soriaga and M. Y. Darensbourg, *J. Am. Chem. Soc.*, 2004, **126**, 12004.
- 27 Z. Wang, J. Liu, C. He, S. Jiang, B. Åkermark and L. Sun, *Inorg. Chim. Acta*, 2007, **360**, 2411.
- 28 A. M. Kluwer, R. Kapre, F. Hartl, M. Lutz, A. L. Spek, A. M. Brouwer, P. W. N. M. Van Leeuwen and J. N. H. Reek, *Proc. Natl. Acad. Sci. U. S. A.*, 2009, **106**, 10460.
- 29 W. Gao, J. Sun, T. Åkermark, M. Li, L. Eriksson, L. Sun and B. Åkermark, *Chem.-Eur. J.*, 2010, **16**, 2537.
- 30 W. N. Cao, F. Wang, H. Y. Wang, B. Chen, K. Feng, C. H. Tung and L. Z. Wu, *Chem. Commun.*, 2012, **48**, 8081.
- 31 F. Quentel, G. Passard and F. Gloaguen, *Energy Environ. Sci.*, 2012, **5**, 7757.
- 32 X. Li, M. Wang, L. Chen, X. Wang, J. Dong and L. Sun, *ChemSusChem*, 2012, **5**, 913.
- 33 B. J. Fisher and R. Eisenberg, *J. Am. Chem. Soc.*, 1980, **102**, 7361.
- 34 R. M. Kellett and T. G. Spiro, *Inorg. Chem.*, 1985, **24**, 2373.
- 35 P. Du, K. Knowles and R. Eisenberg, *J. Am. Chem. Soc.*, 2008, **130**, 12576.
- 36 J. L. Dempsey, B. S. Brunschwig, J. R. Winkler and H. B. Gray, *Acc. Chem. Res.*, 2009, **42**, 1995.
- 37 V. Fourmond, P. A. Jacques, M. Fontecave and V. Artero, *Inorg. Chem.*, 2010, **49**, 10338.
- 38 P. Zhang, M. Wang, J. Dong, X. Li, F. Wang, L. Wu and L. Sun, *J. Phys. Chem. C*, 2010, **114**, 15868.
- 39 C. F. Leung, S. M. Ng, C. C. Ko, W. L. Man, J. Wu, L. Chen and T. C. Lau, *Energy Environ. Sci.*, 2012, **5**, 7903.
- 40 C. C. L. McCrory, C. Uyeda and J. C. Peters, *J. Am. Chem. Soc.*, 2012, **134**, 3164.
- 41 M. Guttentag, A. Rodenberg, C. Bachmann, A. Senn, P. Hamm and R. Alberto, *Dalton Trans.*, 2013, **42**, 334.
- 42 J. P. Collin, A. Jouaiti and J. P. Sauvage, *Inorg. Chem.*, 1988, **27**, 1986.
- 43 A. Begum, G. Moula and S. Sarkar, *Chem.-Eur. J.*, 2010, **16**, 12324.
- 44 M. L. Helm, M. P. Stewart, R. M. Bullock, M. R. DuBois and D. L. DuBois, *Science*, 2011, **333**, 863.
- 45 U. J. Kilgore, J. A. S. Roberts, D. H. Pool, A. M. Appel, M. P. Stewart, M. R. DuBois, W. G. Dougherty, W. S. Kassel, R. M. Bullock and D. L. DuBois, *J. Am. Chem. Soc.*, 2011, **133**, 5861.
- 46 O. R. Luca, S. J. Konezny, J. D. Blakemore, D. M. Colosi, S. Saha, G. W. Brudvig, V. S. Batista and R. H. Crabtree, *New J. Chem.*, 2012, **36**, 1149.
- 47 H. I. Karunadasa, C. J. Chang and J. R. Long, *Nature*, 2010, **464**, 1329.
- 48 Y. Hou, B. L. Abrams, P. C. K. Vesborg, M. E. Björketun, K. Herbst, L. Bech, A. M. Setti, C. D. Damsgaard, T. Pedersen, O. Hansen, J. Rossmeisl, S. Dahl, J. K. Nørskov and I. Chorkendorff, *Nat. Mater.*, 2011, **10**, 434.
- 49 H. I. Karunadasa, E. Montalvo, Y. Sun, M. Majda, J. R. Long and C. J. Chang, *Science*, 2012, **335**, 698.
- 50 A. J. Esswein and D. G. Nocera, *Chem. Rev.*, 2007, **107**, 4022.
- 51 A. Raba, M. Cokoja, S. Ewald, K. Riener, E. Herdtweck, A. Pöthig, W. A. Herrmann and F. E. Kühn, *Organometallics*, 2012, **31**, 2793.
- 52 C. Bachmann, M. Guttentag, B. Spingler and R. Alberto, *Inorg. Chem.*, 2013, **52**, 6055.
- 53 M. Nippe, R. S. Khnayzer, J. A. Panetier, D. Z. Zee, B. S. Olaiya, M. Head-Gordon, C. J. Chang, F. N. Castellano and J. R. Long, *Chem. Sci.*, 2013, **4**, 3934.
- 54 R. S. Khnayzer, C. E. McCusker, B. S. Olaiya and F. N. Castellano, *J. Am. Chem. Soc.*, 2013, **135**, 14068.
- 55 Y. Sun, J. P. Bigi, N. A. Piro, M. L. Tang, J. R. Long and C. J. Chang, *J. Am. Chem. Soc.*, 2011, **133**, 9212.

- 56 K. M. Lam, K. Y. Wong, S. M. Yang and C. M. Che, *J. Chem. Soc., Dalton Trans.*, 1995, 1103.
- 57 W. Zambach, L. Quaranta, C. Massol-Frieh, S. Trah, D. Stierli, M. Pouliot and K. Nebel, Novel Microbiocides, International Publication Number WO2013026866 A2, 2013.
- 58 Precatalytic reduction events are commonly observed for Co based HER catalysts in aqueous media. See references.
- 59 A. E. King, Y. Surendranath, N. A. Piro, J. P. Bigi, J. R. Long and C. J. Chang, *Chem. Sci.*, 2013, **4**, 1578.
- 60 R. S. Khnayzer, L. B. Thompson, M. Zamkov, S. Ardo, G. J. Meyer, C. J. Murphy and F. N. Castellano, *J. Phys. Chem. C*, 2012, **116**, 1429.
- 61 D. R. Anton and R. H. Crabtree, *Organometallics*, 1983, **2**, 855.
- 62 C. R. Bock, J. A. Connor, A. R. Gutierrez, T. J. Meyer, D. G. Whitten, B. P. Sullivan and J. K. Nagle, *J. Am. Chem. Soc.*, 1979, **101**, 4815.
- 63 B. H. J. Bielski, D. A. Comstock and R. A. Bowen, *J. Am. Chem. Soc.*, 1971, **93**, 5624.
- 64 J. Van Houten and R. J. Watts, *J. Am. Chem. Soc.*, 1976, **98**, 4853.
- 65 B. Durham, J. V. Caspar, J. K. Nagle and T. J. Meyer, *J. Am. Chem. Soc.*, 1982, **104**, 4803.
- 66 G. H. Allen, R. P. White, D. P. Rillema and T. J. Meyer, *J. Am. Chem. Soc.*, 1984, **106**, 2613.
- 67 J. Van Houten and R. J. Watts, *Inorg. Chem.*, 1978, **17**, 3381.
- 68 N. Sutin and C. Creutz, in *Inorganic and Organometallic Photochemistry*, American Chemical Society, 1978, vol. 168, pp. 1–27.
- 69 A. Juris, V. Balzani, F. Barigelletti, S. Campagna, P. Belser and A. Von Zelewsky, *Coord. Chem. Rev.*, 1988, **84**, 85.
- 70 K. Kalyanasundaram, *Coord. Chem. Rev.*, 1982, **46**, 159.
- 71 M. Ruthkosky, F. N. Castellano and G. J. Meyer, *Inorg. Chem.*, 1996, **35**, 6406.
- 72 T. E. Mallouk, J. S. Krueger, J. E. Mayer and C. M. G. Dymond, *Inorg. Chem.*, 1989, **28**, 3507.
- 73 S. C. Marinescu, J. R. Winkler and H. B. Gray, *Proc. Natl. Acad. Sci. U. S. A.*, 2012, **109**, 15127.
- 74 E. A. Ünal, D. Wiedemann, J. Seiffert, J. P. Boyd and A. Grohmann, *Tetrahedron Lett.*, 2012, **53**, 54.